Fourier-transform scanning tunneling microscopy investigation of the energy versus wave vector dispersion of electrons at the Au(111) surface

K. Schouteden,* P. Lievens, and C. Van Haesendonck†
Laboratory of Solid-State Physics and Magnetism and Institute for Nanoscale Physics and Chemistry (INPAC), Katholieke Universiteit Leuven, BE-3001 Leuven, Belgium
(Received 13 January 2009; published 11 May 2009)

We have investigated the contributions of surface-state electrons and bulk state electrons to the spatially oscillating local density of states (LDOS) of the Au(111) surface by scanning tunneling microscopy and spectroscopy at low temperatures. Based on the Fourier-transform images of LDOS maps obtained at various energies, we were able to determine the dispersion of the surface-state electrons in a broad range of energies, up to 3 eV. The energy versus wave vector dispersion relation was found to clearly deviate from the parabolic free-electron-like behavior at higher energies above 1 eV. Moreover, relying on two-dimensional Fourier-transform analysis, we develop an original approach to determine the dispersion behavior of bulk state electrons that are scattered at (sub)surface defects in the top atomic layers of the Au(111) surface. This "additional set" of electrons is found to exhibit a dispersion for the occupied states that is consistent with the calculated band structure of bulk Au and previous photoemission experiments. On the other hand, an anomalous bulk state dispersion behavior occurs in the empty state regime, where the wavelength of the spatial oscillations of the LDOS is observed to remain constant for the investigated energy range. This behavior is inconsistent with previous band-structure calculations and requires further theoretical investigation that takes into account the influence of inelastic electron scattering.

DOI: 10.1103/PhysRevB.79.195409 PACS number(s): 73.20.At, 68.37.Ef, 71.20.Be

I. INTRODUCTION

Besides its characteristic topographical features, the Au(111) surface also exhibits remarkable electronic properties that are dominated by its intriguing *sp*-derived Shockley-type surface state. The presence of such a surface state is a typical property of various (111) surfaces, including Cu(111),[1] Ag(111),[2] and Au(111),[3] as well as other surfaces, including NiAl(110)[4] and Be(0001).[5] The Au(111) surface state consists of delocalized electrons that are confined to the top atomic layers of the surface: At one side there is confinement by the vacuum barrier and at the other side by the *sp*-band gap in the bulk valence states.[6] Surface state electrons can therefore be treated as a quasi-two-dimensional (quasi-2D) free-electron gas,[7,8] providing an ideal playground for fundamental physics investigations, such as electron scattering and confinement effects in nanosized quantum corrals,[9,10] islands,[11–13] and vacancy islands[14,15] that are created on these surfaces.

An ideal tool to reliably investigate the properties of surface states is the tunneling microscope since it allows to obtain both local topographic and electronic information. Surface-state electrons are scattered at step edges, defects, and impurities. The resulting interference of the incident and reflected electron waves gives rise to energy-dependent periodic spatial oscillations in the local density of states (LDOS) at the surface, which can be probed by means of scanning tunneling microscopy (STM) and scanning tunneling spectroscopy (STS). This way, STM and STS provide direct experimental access to both the occupied and empty states regime, in contrast to, e.g., angle-resolved photoemission measurements, which can only probe the dispersion of the occupied states.[16] With STM and STS it is thus possible to derive the $E(\vec{k})$ energy versus wave vector dispersion of the surface-state electrons around the Fermi level. This can be achieved by either measuring the wavelength of the standing-wave patterns in the LDOS maps near a step edge[3,17] or, alternatively, from the Fourier-transform (FT) image of the LDOS maps.[5] For (111) surfaces, such a FT image yields a ringlike feature, implying that the surface-state electrons are isotropically scattered in all directions across the surface.[18]

Previously, Petersen *et al.*[18] reported on the observation at low temperatures of an additional concentric ring in the FT image of constant current STM images for both Au(111) and Cu(111) surfaces. However, the authors limited their experiments to standard STM imaging near the Fermi energy, i.e., within a range of voltages of only a few mV around zero bias. The authors ascribed the additional ring to screening waves from electrons with $\vec{k}$ vector in the vicinity of the "neck" of the bulk Fermi surface. The Au Fermi surface has the shape of a sphere in $\vec{k}$ space with "necks" sticking out in the $\langle 111 \rangle$ directions [the Au(111) surface Fermi circle cuts such a neck]. Within this Fermi "neck" bulk states are forbidden.[19] The inner and outer rings in the FT image (of an STM image taken in the occupied state region, just below the Fermi energy) were attributed by Petersen *et al.* to surface and bulk state electrons, respectively. Since both the bulk and surface wave functions contribute to the LDOS at the crystal surface with tails decaying into the vacuum, STM is able to pick up both bulk and surface-state contributions to the tunneling current. This explains why one can observe the screening waves originating from both surface-state and bulk state electrons at the surface. The bulk state electrons are also scattered at (sub)surface defects, resulting in additional complex interference patterns similar to the surface-state electrons. The $E(\vec{k})$ dispersion of this "additional set" of electrons has, however, never been investigated, at least to our knowledge.

LaShell *et al.*[20] previously reported on the observation of two close-lying spin-orbit-splitted surface-state bands by means of angle-resolved photoemission measurements, which may correspond to the two close-lying Fermi contours observed with STM. Based on a 2D tight-binding calculation, Petersen *et al.*[21] recently ruled out this possibility by showing that the interfering electron wave functions, which are mapped with STM, oscillate with the average of the spin-split wave vectors exclusively.

Up until now, the dispersion behavior of the Au(111) surface state has only been investigated at room temperature within a limited range of energies around the Fermi energy, up to a few hundreds of meV.[3] Extensive low-temperature investigations of the Cu(111) and Ag(111) surface state was already performed by Bürgi *et al.*,[22] revealing that the dispersion of the surface-state electrons deviates from the parabolic free-electron-like behavior at higher energies (around 1 eV). Experimental information for Au(111) surfaces is, however, still lacking. Here, we report on our measurements of the Au(111) surface-state dispersion behavior in a broad range of energies up to 3 eV and at low temperatures. We clearly observe a deviation from the free-electron-like behavior. Furthermore, we investigated the dispersion behavior of the contribution of bulk state electrons to the LDOS at the Au(111) surface in a broad energy window by mapping of the LDOS as a function of the bias voltage. We found a paraboliclike behavior below the Fermi level with a strong divergence occurring at the Fermi level.

II. EXPERIMENTAL

Epitaxially grown 140-nm-thick Au(111) films on freshly cleaved mica were prepared by molecular beam epitaxy (MBE) at elevated temperatures.[23] Sample transfer from the MBE setup to the low-temperature ultrahigh-vacuum (UHV) STM setup is performed under ambient conditions. The Au(111) surfaces are cleaned in the preparation chamber of the STM setup by repeated cycles of Ar ion sputtering (at about 4 keV and 10^{-6} mbar) and annealing (at about 720 K). The resulting film surfaces consist of atomically flat islands with dimensions up to 500×500 nm^2.

STM and STS measurements were performed with a low-temperature STM system (Omicron Nanotechnology), operating under UHV conditions at a base pressure in the 10^{-11} mbar range and at low temperatures. For maximum topography and energy resolution, all measurements were performed at low temperatures both at liquid nitrogen ($T_{\text{sample}} \simeq 78$ K) and liquid helium ($T_{\text{sample}} \simeq 4.5$ K) temperature. Mechanically cut *PtIr* (10% *Ir*) tips were used as well as electrochemically etched *W* tips. The latter tips were cleaned *in situ* by repeated flashing well above 1000 K in order to remove the surface oxide layer and additional contamination. STM topographic imaging was performed in constant current mode. Differential conductance images referred to as maps of the LDOS, hereafter, are acquired with closed feedback loop by means of harmonic detection with a lock-in amplifier at modulation frequencies in the 800–4000 Hz range and with modulation amplitudes in the 20–100 mV range. Additionally, $dI/dV(V)$ curves are locally recorded with open feedback loop. The bias voltages indicated in the text and figure captions are with respect to the sample while the STM tip is virtually grounded. Image processing was performed by Nanotec WSXM.[24]

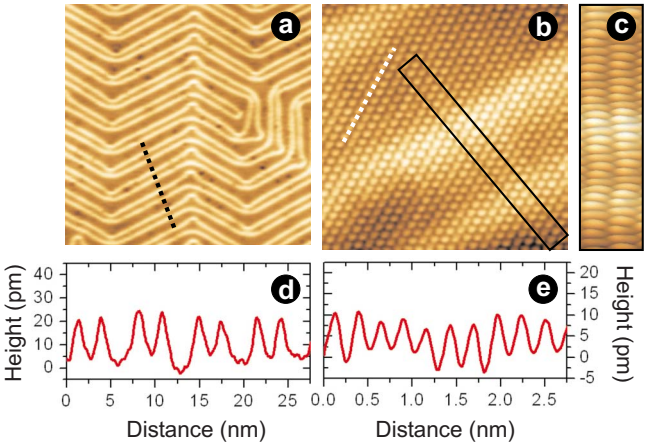

FIG. 1. (Color online) (a) 80.0×80.0 nm^2 and (b) 6.6×6.6 nm^2 constant current STM images of the Au(111) "herringbone" reconstruction and the Au(111) surface atomic structure, respectively. (c) Detailed topographic visualization of the Au(111) surface confined within the black rectangle in (b). (d) and (e) are height profiles taken along the black and white dotted lines in (a) and (b), respectively. $T = 4.5$ K.

Figure 1(a) presents a typical STM topographic image at $T_{\text{sample}} \simeq 4.5$ K of the reconstructed Au(111) surface after the *in situ* cleaning procedure. From the height profile in Fig. 1(c) [taken along the black dotted line in (a)] it can be seen that the ridges are "squeezed out" by only 10–20 pm.[25] The broader regions (3.8 nm) between the ridges are known to have fcc stacking, while the narrower regions (2.5 nm) exhibit hcp stacking [see Fig. 1(b)]. This remarkable reconstruction with zigzag alternating line features is commonly referred to as the Au(111) "herringbone" reconstruction. The atomic corrugation [Fig. 1(e)] of the hexagonal (111) lattice [Fig. 1(b)] is on the same order of magnitude as the "herringbone" related height variations [Fig. 1(d)].[26] The difference between the fcc and hcp regions can be observed at the surface, as illustrated in Fig. 1(c), which is a detailed topographic visualization of the Au(111) surface confined by the black rectangle in Fig. 1(b). When compared to the atoms in the fcc stacking region, the atoms in the hcp region are slightly shifted (by only a few tens of pm) in the direction parallel to the ridges.[25,27]

III. ELECTRONIC SURFACE STATE

The interference patterns resulting from scattering of surface-state electrons are nicely illustrated for the Au(111) monatomic step edge in Fig. 2(a) and the corresponding LDOS map in Fig. 2(b) taken at +150 meV. Brighter features correspond to a higher LDOS, while darker features correspond to a lower LDOS. It is clear that close to the step edge, the standing waves run perpendicular to the step, while circular isotropic patterns are formed in the vicinity of (sub) surface defects. It is noteworthy that the step edge acts as a

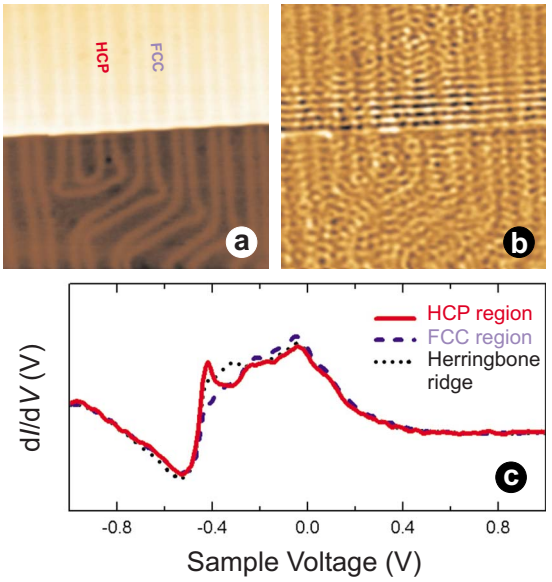

FIG. 2. (Color online) (a) 41.0×41.0 nm^2 constant current image of a monatomic Au(111) step and (b) the corresponding LDOS map at +150 meV. Standing-wave interference patterns arise from electron scattering at the step edge, surface defects, and impurities (T=78 K). (c) dI/dV curves of Au(111) reveal a steplike onset around −460 meV, the signature of the surface-state. The hcp region contains a higher density of lower-energy electrons while the fcc region contains more higher-energy electrons (T=4.5 K).

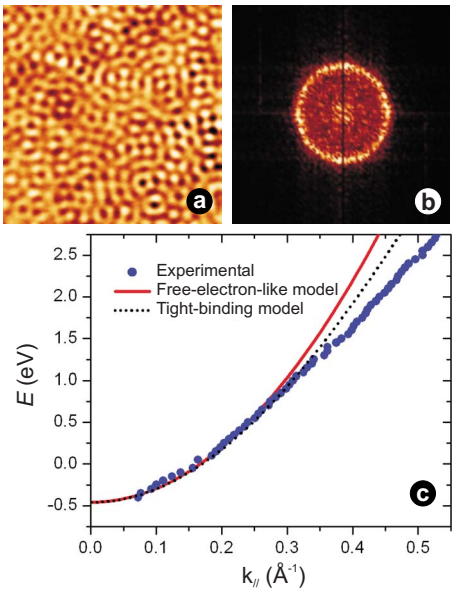

FIG. 3. (Color online) (a) 35.3×35.3 nm^2 LDOS map at −30 meV of an Au(111) terrace (T=78 K). (b) The corresponding 2.5×2.5 nm^{-2} FT image indicates that only a narrow range of wave vectors contributes to the observed standing-wave patterns. (c) Plot of the electron energy E as a function of the parallel wave vector $k_{\|}$, as determined from the FT image of LDOS maps taken at different bias voltages V (T=4.5 K). Experimental results are fitted to the free-electron-like model as well as to a tight-binding model.

strong scatterer with a high reflection coefficient for the electrons on the upper terrace, while the electrons on the lower lying terrace apparently are much more weakly scattered. This can be explained by the fact that electrons move freely within the same Au(111) atomic layer.[28] Electrons at the lower part of the step edge are therefore only slightly affected by the step edge when compared to electrons at the upper part and simply move "underneath" the step edge instead of being strongly reflected by it. Alternatively, it was argued by Avouris and Lyo[29] that electrons incident at the lower side of the step are more easily transmitted to bulk empty states by scattering at the step edge and therefore show less-pronounced standing-wave patterns. We also note that the reconstruction ridges are weakly visible in the LDOS map, implying that they have a slightly higher electron density compared to the surrounding surface.[30]

The Au(111) surface state cannot only be observed via the standing waves in LDOS maps but also in local dI/dV versus V spectra. A sudden increase in tunneling conductance around −460 meV is the well-known signature of the Au(111) surface state.[30] Other (111) surfaces such as Ag(111) and Cu(111) exhibit a similar surface state around −65 meV (Ref. 11) and −450 meV (Ref. 7), respectively. As shown by Chen *et al.*,[30] $dI/dV(V)$ measurements can even distinguish between the wider fcc and the smaller hcp regions of the reconstructed surface. As illustrated in Fig. 2(c), lower-energy electrons favor the hcp regions, whereas the fcc regions are populated by an excess of higher-energy electrons. This specific electronic feature of the Au(111) surface state confirms the quality of our STS measurements.

Since the standing waves occur isotropically along all directions on the surface with similar wavelengths, the surface electron state gives rise to a circular 2D contour in the FT image.[5] This is visualized in Fig. 3(a), presenting a LDOS map at −30 meV of a flat terrace, several nanometers away from any step edge. The corresponding FT image in Fig. 3(b) reveals a quasiperfect circular Fermi contour, indicating that one single wavelength is dominating the standing-wave formation. Based on the FT images of LDOS maps obtained at various bias voltages V, the energy dispersion relation $E(\vec{k}_{\|})$ of the Au(111) surface state can be constructed. By taking the radial average of the FT images, a value of the parallel part $k_{\|}$ of the wave vector $\vec{k}=\vec{k}_{\perp}+\vec{k}_{\|}$ is obtained at each applied bias voltage V for electrons with energy $E(\vec{k}_{\perp},\vec{k}_{\|})=E_F+eV$.[31] We need to take into account that the obtained radial average corresponds to twice the wave vector $k_{\|}$ since the STM measurements map the square of the electron wave function. Figure 3(c) gives an overview of the thus obtained data. Measurements with different tips on different Au(111) film surfaces yielded similar results at both 78 and 4.5 K. We did not attempt to extract the dispersion data at room temperature as thermal drift of the piezoscanner erroneously causes the Fermi circle to be ellipsoidal,[32,33] thereby hampering an accurate wavelength determination.

As can be seen in Fig. 2(c), the surface state only "starts" at −460 meV: no interference patterns are resolved below this energy, only reconstruction and defect related features can be observed. Above this energy the wave patterns can be clearly observed. With increasing energy the LDOS oscillation amplitudes decrease imposing an upper limit on our

measurement window. Nevertheless, we were able to extract $k_{\|}$ values up to energies as high as +2750 meV, which is far beyond the maximum energy reported so far for Au(111), at least to our knowledge.[3] The $E(k_{\|})$ relation around the Fermi level is consistent with the expected parabolic behavior of a quasi-2D free-electron-like gas, where the free-electron mass m_e is replaced by the effective electron mass m^* to take into account the surface electron band structure.[34] The solid line shown in Fig. 3(c) is a fit of the experimental data to the parabolic dispersion relation

$$E(k_{\|}) = E_0 + \hbar^2 k_{\|}^2 / 2m^*, \tag{1}$$

where E_0 is the onset energy of the surface state. Fitting values are -460 ± 5 meV for E_0 and 0.23 ± 0.03 for m^*/m_e. Both values are in reasonable agreement with previously reported values obtained from LDOS maps [$E_0 = -450$ meV and $m^*/m_e = 0.15$ (Ref. 3)] and with photoelectron spectroscopy [$E_0 = -487$ meV and $m^*/m_e = 0.255$ (Ref. 35)]. For higher energies above +750 meV, however, there appears a significant deviation of the experimental data from the free-electron-like parabola. It is observed that the dispersion becomes more or less linear and thus bends away from the parabola with increasing $k_{\|}$. Bürgi *et al.*[22] reported similar deviations from parabolic behavior for Ag(111) and Cu(111) surfaces, and they proposed an alternative model to explain the experimental observations. It was argued that since the effective electron mass m^* considerably deviates from the free-electron mass m_e, the influence of the crystal potential is rather strong, implying that one cannot apply the nearly free-electron approximation for extended $k_{\|}$ ranges. Therefore, Bürgi *et al.* opted for a simple tight-binding model, which was able to account for the dispersion deviating at higher energies by considering a single *s* band in an infinite lattice cleaved along the crystallographic (111) plane of an fcc crystal. Based on the formalism presented in Ref. 36, Bürgi *et al.* relied on the surface-state dispersion relation

$$E(k_x, k_y) = E_0 + \gamma \left[3 - \cos(k_y a) - 2 \cos\left(\frac{k_y a}{2}\right) \cos\left(\frac{\sqrt{3} k_x a}{2}\right) \right], \tag{2}$$

where γ (determines the bandwidth of the surface state) was used as a fitting parameter, yielding 1.6 eV and 1.8 eV for Ag(111) and Cu(111), respectively. Here, we find that for the case of Au(111) a γ value of 2.6 eV yields the best fit of the dispersion data using Eq. (2) [see Fig. 3(c)]. The tight-binding model clearly reproduces more accurately the experimental data at least up until the inflexion point around 1500 meV. A similar behavior was observed before for Ag(111).[22] Our measurements confirm that the free-electron picture for the surface-state band structure is valid within a restricted energy range around the Fermi level. The high-energy unoccupied states, however, deviate from this free-electron-like dispersion, which can to some extent be accounted for by the influence of the crystal potential. The additional deviations from parabolic behavior at the highest energies may be accounted for by the finite height of the tunneling barrier (typically around 4–5 eV for metals[37]). Electrons with a higher energy (and thus larger $\vec{k}$ vector) have a higher tunneling transmission probability when compared to electrons near the Fermi energy,[38,39] causing deviation from the theoretical dispersion relation given by Eq. (2).

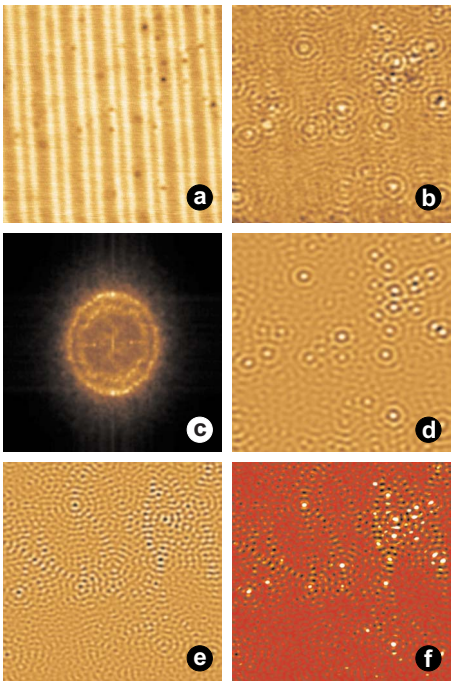

FIG. 4. (Color online) (a) 40.0×40.0 nm^2 constant current image of a Au(111) terrace. (b) LDOS map of the terrace in (a) recorded at +400 meV ($T = 78$ K). (c) The corresponding 4.1 $\times 4.1$ nm^{-2} FT image of (b) reveals that two different wavelengths are contributing to the standing-wave patterns in (b). (d) Inverse FT image of the inner ring in (c). (e) Inverse FT image of the outer ring in (c). (f) Same as (e) but with the "bright scattering centers" appearing in (d) added to the image as bright spots.

IV. CONTRIBUTION FROM BULK STATES

In addition to the circular contour in the FT image of interfering surface-state electrons, we observed an extra concentric ring that also varied as a function of the applied sample voltage. This means that for each electron energy, two sets of standing-wave patterns with different wave vector are present in the LDOS maps. Close to the Fermi level E_F, however, it is very difficult to discern the two contours in the FT image since they (partially) overlap each other [see Fig. 3(b)]. Both contours appear to exhibit a different energy dependence, implying that at energies well above or below the Fermi level E_F the presence of the additional contour becomes more evident. This is illustrated in Fig. 4. Figure 4(b) presents a LDOS map (taken at +400 meV) of the atomically flat Au(111) region shown in Fig. 4(a). The corresponding FT image in Fig. 4(c) clearly reveals the presence of two concentric contours. We have observed this phenomenon in all our measurements at $T = 4.5$ K as well as $T = 78$ K on different Au(111) substrates using both *PtIr* and *W* tips and at various settings of the lock-in frequency and amplitude (see Sec. II). Figure 5 presents the $E(k_{\|})$ dispersion relation of the "additional set" of standing waves. The data

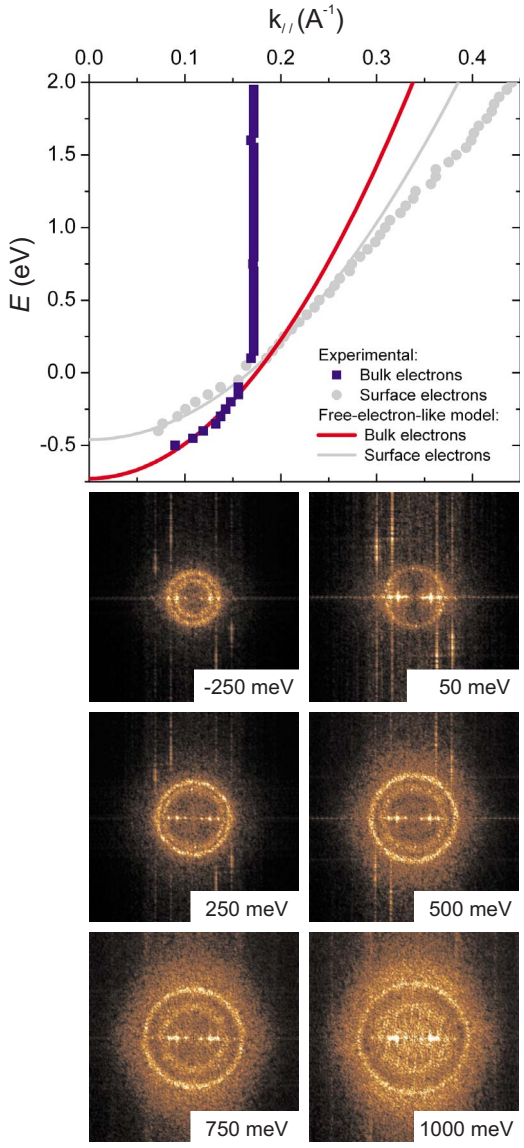

FIG. 5. (Color online) Dispersion behavior of the bulk state electrons (T=4.5 K). The 3.8×3.8 nm^{-2} FT images illustrate the different dispersion behavior of the two sets of standing waves (T =4.5 K). Results below the Fermi level are fitted to the free-electron-like parabolic dispersion relation. Results for the surface-state electrons [see Fig. 3(c)] are added as a reference in gray color.

of Fig. 3(c) for the surface-state electrons are added as a reference to Fig. 5. The different dispersion of the two standing-wave sets is clearly visible in the FT images at different energies that are presented in the lower part of Fig. 5.

As already discussed in the introduction, the additional contour in the FT images has been attributed before to the contribution of bulk state electrons to the LDOS at the Au(111) surface. Below the Fermi level the inner and the outer ring can be assigned to surface and bulk state electrons, respectively. On the other hand, above the Fermi level the outer and the (less pronounced) inner ring are addressed to surface and bulk state electrons, respectively. Although it is not *a priori* clear whether either the inner or outer ring should be linked to the surface or bulk contribution, it is obvious from Fig. 5 that the dispersion data, which we assign to bulk state electrons, deviates strongly from the data for the surface-state electrons, both above and below the Fermi level.

In order to visualize more clearly the contribution of each standing-wave set to the LDOS map in Fig. 4(b), one can take the inverse FT image of each of the concentric rings in Fig. 4(c) separately. Figures 4(d) and 4(e) show the contribution in real space of the inner and the outer contour, respectively. It appears that the inverse FT of the contours addressed as bulk contributions [Fig. 4(d)] reveal a maximum at what seems to be the scattering centers [corresponding to tiny "depressions" in Fig. 4(a)], while the surface contributions [Fig. 4(e)] exhibit a minimum at these locations. This observation can be used as an additional indication to distinguish between a contour stemming from surface or bulk state electrons. Related to this, it should be noted that the majority of scattering centers in Fig. 4(d) appears to act as a scattering center in Fig. 4(e) as well. This is visualized more clearly in Fig. 4(f), which is created by "adding" the scattering centers in Fig. 4(d) as bright spots to Fig. 4(e). This indicates that both surface-state and bulk state electrons are to some extent scattered by the same (sub)surface defects and that both states are coupled to each other by scattering of surface states into bulk states and vice versa.

By further careful comparison of Figs. 4(d) and 4(e) it can be seen that the amplitude of the bulk state-related oscillations decays faster than that of the surface-state-related oscillations. As discussed by Petersen *et al.*,[18] this can be expected since the amplitude of these Friedel-type oscillations decays with the distance r from the scatterer as $1/r^{a-1}$, where $a>0$ depends on the dimensionality of both the electron gas and the scatterer and is generally larger for three-dimensional (3D) screening than for 2D screening.

Remarkable in Fig. 5 is the abrupt change in the bulk state dispersion behavior at the Fermi level E_F. Below E_F the data follow a paraboliclike behavior, which we have fitted using Eq. (1) with $E_0=-720\pm3$ meV and $m^*/m_e=0.16\pm0.01$. Relying on the approach introduced by Petersen *et al.*, the contour related to the bulk state electrons should correspond to a broadened or blurred circle with radius corresponding to the minimum value of $k_\parallel$ that is allowed by the *sp*-related band gap in the bulk density of states [see Eq. (4) in Ref. 18]. This minimum value can be extracted from the bulk band structure after projection for the (111) surface. Details of this projected band structure were provided by Kevan and Gaylord[16] based on photoelectron spectroscopy. Table I in Ref. 16 indicates that the dispersion for the *sp*-derived band-gap edge corresponds to an effective mass $m^*/m_e=0.21\pm0.01$ and an onset energy $E_0=-900\pm30$ meV. We conclude that for the occupied states, our experimental results related to the bulk electron states of Au are in reasonable agreement with the band-structure data reported in Ref. 16.

At E_F, however, our experimentally determined dispersion for the bulk electron states suddenly diverges. For all positive applied bias voltages, the bulk state-related contour exhibits a radius that remains equal to that at E_F within the accuracy of the measurement. Assuming we can continue to use Eq. (4) in Ref. 18 for interpreting our data above the Fermi energy, the observed electron standing-wave patterns

indicate that the minimum value of $k_{\|}$ for the projected bulk states becomes a constant above the Fermi energy, i.e., remains equal to the radius k_{neck} of the "neck" that sticks out of the Fermi surface in the $\langle 111 \rangle$ directions. This is clearly inconsistent with the projected band structure that is continuous at the Fermi energy for the noble metals.[19] We then come to the conclusion that an analysis of our results in terms of Eq. (4) in Ref. 18 no longer holds for energies above the Fermi energy.

It is likely that the anomaly that occurs above the Fermi energy is somehow related to very different inelastic relaxation rates for electron states that are above and below the Fermi level.[40] A possible explanation for our observations can be based on the theoretical findings of Becker *et al.*[41] These authors reported on theoretical calculations of the Ag(111) surface state and concluded that there is a rapidly increasing decay rate for surface electron states with increasing energy above the Fermi level. This decay rate depends on the coupling between surface state and bulk states and is expected to dominate the recorded LDOS maps when the rate becomes comparable to the tunneling rate. The electron injection into the Au(111) bulk states above the Fermi level, which occurs for positive sample bias voltages, is hampered by the extended projected bulk band gap.[16] Two-electron processes involving excitation of an electron-hole pair at E_F could provide the momentum transfer for the tunneling electron to enter into allowed states with large $k_{\|}$. It appears plausible that the probability for such a process scales with the LDOS at E_F. Further theoretical investigation, which is beyond the scope of the present work, is required to clarify the observed dispersion for bulk state electrons.

V. CONCLUSIONS

By means of low-temperature scanning tunneling microscopy and spectroscopy under ultrahigh-vacuum conditions we were able to determine the energy dispersion relation $E(k_{\|})$ of the Au(111) surface electron state for a broad range of energies of up to 3 eV. Our measurements verify that the free-electron picture of the surface-state band structure is valid for an energy range of several hundreds of meV around the Fermi level. It was observed, however, that the high-energy unoccupied states clearly deviate from this free-electron-like dispersion. This can be accounted for by the influence of the crystal potential and the finite height of the tunneling barrier. Furthermore, we have systematically investigated the energy dependence of the contribution of bulk state electrons to the electron standing-wave patterns at the Au(111) surface. A $E(k_{\|})$ dispersion relation was inferred for the occupied state regime that is consistent with the project bulk band structure projected for the (111) surface. On the other hand, an anomalous and very strong divergence of unknown origin occurs at the Fermi level requiring further theoretical investigation.

ACKNOWLEDGMENTS

This work has been supported by the Fund for Scientific Research – Flanders (Belgium) as well as by the Belgian Interuniversity Attraction Poles (IAP) and the Flemish Concerted Action (GOA) research programs.

*koen.schouteden@fys.kuleuven.be
†http://fys.kuleuven.be/

[1] G. Hörmandinger, Phys. Rev. B **49**, 13897 (1994).
[2] J. Li, W. Schneider, S. Crampin, and R. Berndt, Surf. Sci. **422**, 95 (1999).
[3] Y. Hasegawa and Ph. Avouris, Phys. Rev. Lett. **71**, 1071 (1993).
[4] K. H. Hansen, J. Gottschalck, L. Petersen, B. Hammer, E. Lægsgaard, F. Besenbacher, and I. Stensgaard, Phys. Rev. B **63**, 115421 (2001).
[5] P. T. Sprunger, L. Petersen, E. E. Lægsgaard, and F. Besenbacher, Science **275**, 1764 (1997).
[6] W. Shockley, Phys. Rev. **56**, 317 (1939).
[7] M. F. Crommie, C. P. Lutz, and D. M. Eigler, Nature (London) **363**, 524 (1993).
[8] L. Bürgi, N. Knorr, H. Brune, M. A. Schneider, and K. Kern, Appl. Phys. A: Mater. Sci. Process. **75**, 141 (2002).
[9] M. F. Crommie, C. P. Lutz, and D. M. Eigler, Science **262**, 218 (1993).
[10] V. S. Stepanyuk, N. N. Negulyaev, L. Niebergall, R. C. Longo, and P. Bruno, Phys. Rev. Lett. **97**, 186403 (2006).
[11] J. Li, W.-D. Schneider, R. Berndt, and S. Crampin, Phys. Rev. Lett. **80**, 3332 (1998).
[12] L. Diekhöner, M. A. Schneider, A. N. Baranov, V. S. Stepanyuk, P. Bruno, and K. Kern, Phys. Rev. Lett. **90**, 236801 (2003).
[13] K. Schouteden, E. Lijnen, E. Janssens, A. Ceulemans, L. F. Chibotaru, P. Lievens, and C. Van Haesendonck, New J. Phys. **10**, 043016 (2008).
[14] H. Jensen, J. Kröger, R. Berndt, and S. Crampin, Phys. Rev. B **71**, 155417 (2005).
[15] L. Niebergall, G. Rodary, H. F. Ding, D. Sander, V. S. Stepanyuk, P. Bruno, and J. Kirschner, Phys. Rev. B **74**, 195436 (2006).
[16] S. D. Kevan and R. H. Gaylord, Phys. Rev. B **36**, 5809 (1987).
[17] J. I. Pascual, A. Dick, M. Hansmann, H.-P. Rust, J. Neugebauer, and K. Horn, Phys. Rev. Lett. **96**, 046801 (2006).
[18] L. Petersen, P. Laitenberger, E. Lægsgaard, and F. Besenbacher, Phys. Rev. B **58**, 7361 (1998).
[19] N. W. Ashcroft and N. D. Mermin, *Solid State Physics* (Saunders, Philadelphia, 1976).
[20] S. LaShell, B. A. McDougall, and E. Jensen, Phys. Rev. Lett. **77**, 3419 (1996).
[21] L. Petersen and P. Hedegård, Surf. Sci. **459**, 49 (2000).
[22] L. Bürgi, L. Petersen, H. Brune, and K. Kern, Surf. Sci. **447**, L157 (2000).
[23] N. Vandamme, E. Janssens, F. Vanhoutte, P. Lievens, and C. Van Haesendonck, J. Phys.: Condens. Matter **15**, S2983 (2003).
[24] I. Horcas, R. Fernandez, J. M. Gomez-Rodriguez, J. Colchero, J. Gomez-Herrero, and A. M. Baro, Rev. Sci. Instrum. **78**, 013705 (2007).
[25] C. Wöll, S. Chiang, R. J. Wilson, and P. H. Lippel, Phys. Rev. B

39, 7988 (1989).
[26] V. M. Hallmark, S. Chiang, J. F. Rabolt, J. D. Swalen, and R. J. Wilson, Phys. Rev. Lett. **59**, 2879 (1987).
[27] J. V. Barth, H. Brune, G. Ertl, and R. J. Behm, Phys. Rev. B **42**, 9307 (1990).
[28] P. M. Echenique, J. Osma, M. Machado, V. M. Silkin, E. V. Chulkov, and J. M. Pitarke, Prog. Surf. Sci. **67**, 271 (2001).
[29] P. Avouris and I. W. Lyo, Science **264**, 942 (1994).
[30] W. Chen, V. Madhavan, T. Jamneala, and M. F. Crommie, Phys. Rev. Lett. **80**, 1469 (1998).
[31] L. Petersen, P. T. Sprunger, Ph. Hofmann, E. Lægsgaard, B. G. Briner, M. Doering, H.-P. Rust, A. M. Bradshaw, F. Besenbacher, and E. W. Plummer, Phys. Rev. B **57**, R6858 (1998).
[32] D. Fujita, K. Amemiya, T. Yakabe, H. Nejoh, T. Sato, and M. Iwatsuki, Surf. Sci. **423**, 160 (1999).
[33] L. Petersen, L. Bürgi, H. Brune, F. Besenbacher, and K. Kern, Surf. Sci. **443**, 154 (1999).
[34] D. J. Griffiths, *Introduction to Quantum Mechanics* (Prentice-Hall, Englewood Cliffs, NJ, 1995).
[35] F. Reinert, G. Nicolay, S. Schmidt, D. Ehm, and S. Hüfner, Phys. Rev. B **63**, 115415 (2001).
[36] D. Kalkstein and P. Soven, Surf. Sci. **26**, 85 (1971).
[37] L. Olesen, M. Brandbyge, M. R. Sørensen, K. W. Jacobsen, E. Lægsgaard, I. Stensgaard, and F. Besenbacher, Phys. Rev. Lett. **76**, 1485 (1996).
[38] R. Wiesendanger, *Scanning Probe Microscopy and Spectroscopy: Methods and Applications* (Cambridge University Press, England, 1994).
[39] J. G. Simmons, J. Appl. Phys. **34**, 1793 (1963).
[40] A. Depuydt, C. Van Haesendonck, N. S. Maslova, V. I. Panov, S. V. Savinov, and P. I. Arseev, Phys. Rev. B **60**, 2619 (1999).
[41] M. Becker, S. Crampin, and R. Berndt, Phys. Rev. B **73**, 081402(R) (2006).